# VERIFICATION OF LUMINOSITY CLASSES FOR SUSPECTED FAINT RED GIANT STARS

Ball State University Honors Thesis (Honors 499)

by

Jason E. Matney

Advisor: Dr Thomas Robertson

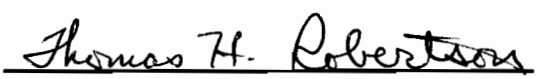

Ball State University
Muncie, IN

December 2004

**Abstract:**

This project is using CCD images taken through different filters to determine the reliability of luminosity classifications based on objective-prism spectra. Kron-Cousins R and I filters are used in conjunction with an intermediate-band calcium hydride (CaH) filter to create a two-color plot. CaH-r vs. R-I diagrams. These are used to photometrically distinguish between red giants and dwarfs. The objective-prism plates from which this sample has been derived are currently being scanned to identify a much larger group of faint red stars. Accurate determinations of the luminosity classes for these sample stars would allow a more objective evaluation of the reliability of luminosity classes for stars detected in this larger survey.

Photometric data taken at the National Undergraduate Research Observatory (NURO) and the Ball State University Observatory are combined in this study. Data gathered to date shows that the giant classification is much more reliable than the dwarf classification based on objective-prism spectral classification. Data collected to date will be reviewed in the context of the overall sample of faint red giant stars.

**Acknowledgements:**

Some data for this project were obtained at the Lowell Observatory 0.78 m telescope, which, under an agreement with Northern Arizona University and the NURO Consortium, is operated 33% of the time as the National Undergraduate Research Observatory. The Indiana Space Grant Consortium, the National Science Foundation/Ball State REU Program, and the Ball State Honors College Undergraduate Fellowship Program have all provided major funding for this project over the past four years.

I would like to acknowledge the Ball State University Physics Department faculty for their hours of hard work, which has imparted the knowledge needed to understand the physical concepts behind this project. Each member of the faculty has beneficially impacted my undergraduate career, and for that, I am thankful.

I would like to especially thank Dr. David Ober, Chairman of the Physics and Astronomy Department, for his guidance and advice during the past five years. It was his contagious enthusiasm that convinced me to initially attend Ball State University.

I would like to thank Jason Croy, Robert Seaton, Steven Poweska, (Ball State undergraduates), Luke Snyder and Fred Welsh (Ball State graduate students) for their assistance in data acquisition and reduction during this project.

I reserve my deepest thanks to my advisor, Dr. Thomas Robertson, in his guidance and support throughout the past four years of research pertaining to this project. I would like to thank him for providing me with my first opportunity for research, and for fostering my interest and passion for astronomy.

# Table of Contents:

# List of Figures and Tables:

Figures:



Tables:

# I. Introduction:

Low luminosity stars are important for many reasons. These relatively cool, low mass stars are estimated to be about 85% of the local star population. These stars have masses that typically range from 8-70% of our own sun's mass. Despite their low masses, they constitute nearly half of the mass of the galaxy since they appear in such high numbers. Therefore, precise determinations of their space densities and kinematic properties are essential for a complete understanding of our galaxy (Robertson and Furiak, 1995). Such a star's lifetimes may range from 30 gigayears to a few terayears. Virtually every star of this type ever formed still exists. Locked away with these often-overlooked stars is the dynamical and chemical history of the Milky Way from birth to present times (Krawchuk, Dawson & De Robertis, 2000). Due to this fact, we must study this faint, but numerous, family of stars to completely understand our galaxy.

Historically, these stars have not been studied in great detail, and this is due to several problems. The most obvious problem is that the stars are very faint. There is not a single target star in this study that is visible with the naked eye. The faint nature of these stars makes it difficult to accurately study these stars. It takes a longer exposure to image these faint stars; thus astronomers with limited time often overlook them. Other problems arise in the fact that heavy molecules exist in the cooler atmospheres that are absent in hotter stars, which complicate the optical and near infrared spectra. (Krawchuk, Dawson & De Robertis, 2000)

## II. Project Overview

At Ball State University, Dr. Robertson has pioneered a new system of photometry, or luminosity classification, that distinguishes between red giant and red dwarf stars using various telescope filters, including a special Calcium-Hydride (CaH) filter. In previous years, Drs. Robertson and Jordan have collected a large sample of stars, which were originally determined, by a quicker method called objective-prism spectral classification, to be either a suspected giant or dwarf star by looking at the star's spectra.

Several BSU students have conducted studies on the suspected dwarf stars. No extensive analysis of the giant sample had been concluded. These suspected giant stars are the target stars of this project.

This project involves using new CaH photometry to verify that stars designated as giant stars are indeed of the giant luminosity class. This will help us determine the reliability of Jordan and Robertson's earlier classification method. The paper will describe the background of the project, the process used to identify and observe the stars, the basics of CaH photometry, and the results/conclusions we have obtained thus far.

## III. Sample Selection

Drs. Robertson and Jordan at Ball State University have collected objective-prism plates of 24 of the Kapteyn Selected Areas. Suspected dwarfs and giants were picked out of this large group in an attempt to identify red stars which might serve to extend traditional standard star lists to redder colors. The

selected stars were classified as either Selected Area Giants or Dwarfs (SAG and SAD respectively). This survey is described in detail in Robertson and Jordan, 1987. Figure 1 shows the visual magnitudes of the SAG sample.

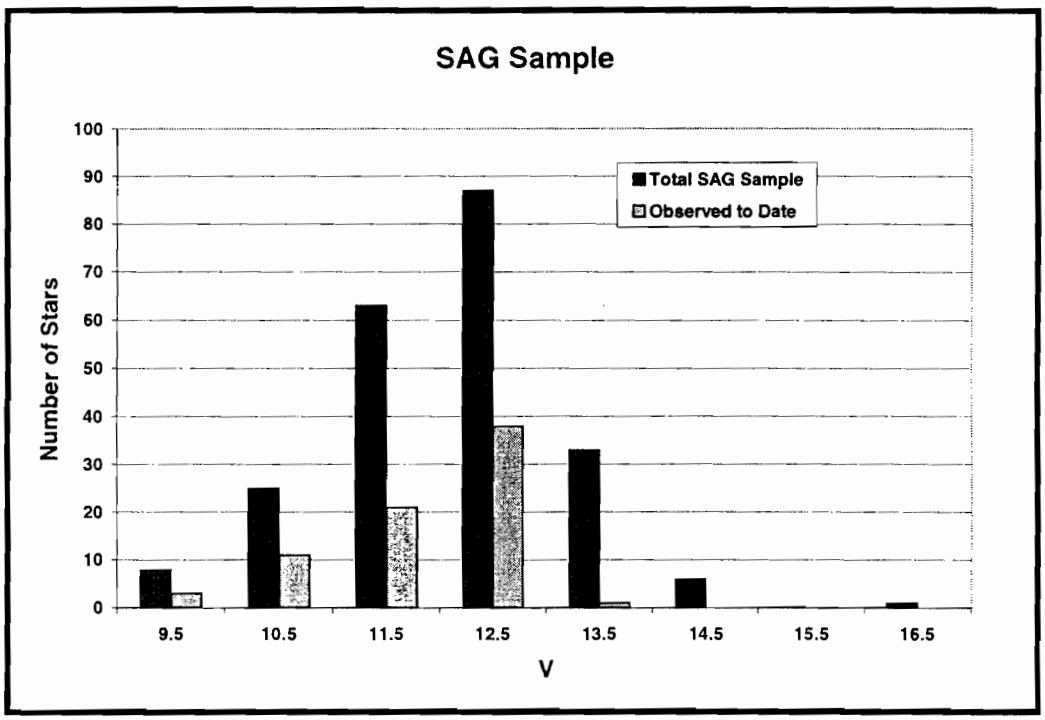


**Figure 1: Breakdown of Visual Magnitudes of the SAG sample**

Several BSU students have conducted studies on the dwarf branch. Richard Maupin completed his master's thesis on his intensive study of the SAD list in 2002. Yet, no extensive analysis of the Selected Area Giant sample had been concluded. These suspected giant stars are the target stars of the project. When a sufficient amount or data has been collected, the reliability of the initial classification will be known. This will allow for the correct interpretation of the reliability of luminosity classes determined from the objective-prism plates. Figure

2 shows the breakdown of the SAG sample by spectral type. Most stars from the SAG list have a spectral classification between M2 and M5.

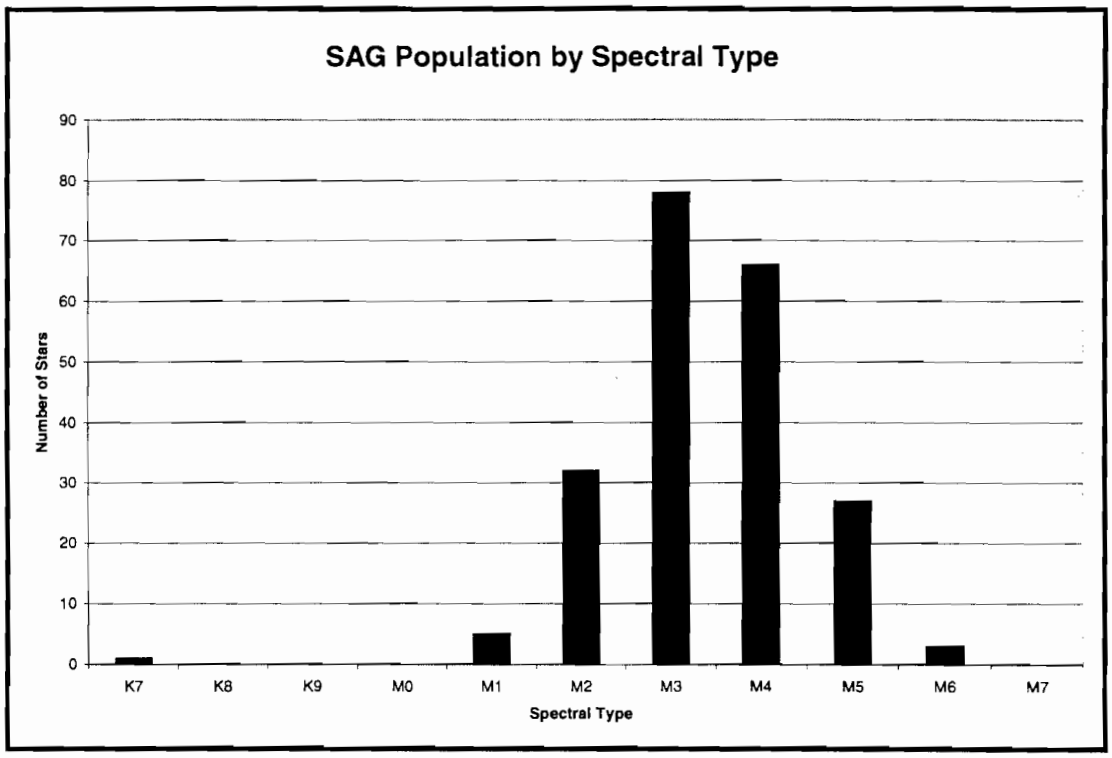


**Figure 2: Breakdown of Spectral Classifications of SAG List**

Figure 3 shows the galactic distribution of the SAG star sample. Except for the fields at higher north galactic latitudes, we have representative samples for most SAG fields. One would expect that giant stars will be more frequent among the brighter stars and dwarf stars will be more frequent among the fainter stars at intermediate and high galactic latitudes. A little more than half (52%) of the SAG sample is within 15 degrees of the galactic plane. (Matney, et al. 2004).

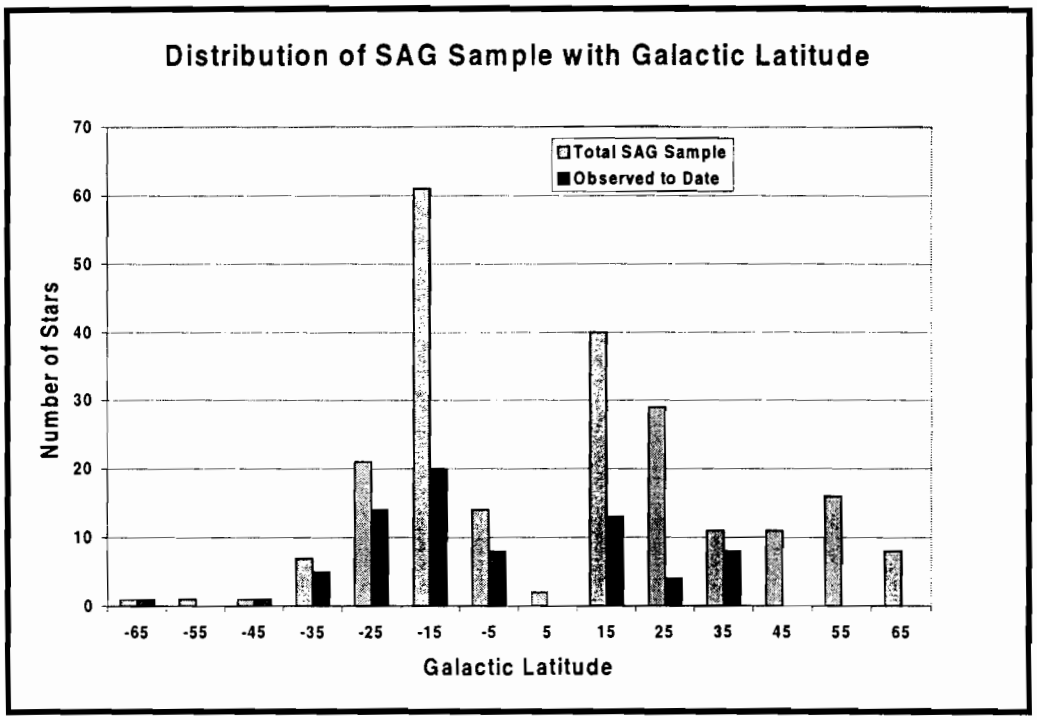


**Figure 3: Distribution of SAG Sample in our galaxy**

In addition to observing our program stars, observations of standard stars selected from the lists of Landolt (1983 and 1992) were taken every night. This allowed us to later transform all magnitudes onto a standardized scale for accurate evaluation and comparison of all data to previously known values.

## IV. Data Acquisition

Images of program and standard stars were acquired at the National Undergraduate Research Observatory (NURO) at Flagstaff, Arizona and at the Ball State University Observatory (BSUO) located on the roof of Cooper Science Building, Muncie, Indiana.

At Ball State, observational data were acquired using the BSUO's 0.35-meter Celestron Schmidt-Cassegrain telescope. A Photometrics Star 1 CCD camera, with 384 by 576 pixels, is used to record the images. This camera is equipped with a water-cooled system that reaches an operating temperature near –45 degrees Celsius. A filter wheel allows us to utilize the Red (R), Visual (V) and Infrared (I) filters, along with our unique Calcium Hydride (L) filter. Table 1 displays information on the various filters that were used during this project.

| | NURO Filters Used |
|---|---|
| Visual (V) | 2mm GG495 + 2mm BG39 |
| Red (R) | 2mm OG570 + 3mm KG3 |
| Infrared (I) | 3mm RG9 + 2mm WG305 |
| Calcium Hydride (L) | Central wavelength at 686 nm, fwhm of 13nm |

**Table 1: Filter Specifications (V, R, and I filter information taken from http:// http://www.nuro.nau.edu/nuro/info/filters.html)**

The NURO observatory is equipped with a 0.8-meter Cassegrain telescope, owned by the Lowell Observatory, and is located on the Anderson Mesa south of Flagstaff, Arizona. The NURO telescope is equipped with a liquid nitrogen cooled Photometrics CCD camera which produces images that are 512 by 512 pixels. The liquid nitrogen cooling system cools the camera to an operating temperature near –110 degrees Celsius. The telescope is fitted with a filter wheel, allowing us to use similar V, R, I, and L filters as at the BSUO.

To begin a typical night of observing at BSUO and NURO, we take three different types of images used to calibrate the images of our target stars. First we obtain fifty or more zero-second-exposures, called bias images. These serve to record a zero point offset present in every image, so that an average value, or a

zero point correction, for each pixel is subtracted from each of our images taken later. Between three and five images are taken without even opening the camera shutter, which are called dark images. These exposures last up to 5 minutes, and serve to record and correct any built up electrical signal due to thermal ionization dependant on temperature. These are scaled with exposure time, so that we may subtract this "dark" thermal background noise from every image, regardless of the exposure time for the image. At NURO, due to the extremely low temperatures (-110 Celsius) at which the camera operates, it is often unnecessary to correct our raw data with dark images. To verify this, dark images are still taken to confirm that dark counts are insignificant.

Next we must take several short-exposure images of the sky during twilight that are referred to as flat field images. These are taken during twilight as the sun sets because we want to obtain images with a uniform background illumination. This serves to measure relative efficiencies of each pixel, vignetting (changes due to pixels located near the edge of the camera), and dust settled within the camera. We later compensate for these imperfections by correcting the image by dividing object frames by the normalized flat field frame. Flat field images vary for each filter, due to the fact we are viewing the target through a different filter, each with its own accumulated dust and debris. Therefore, we must take several flat field images for each filter used during the observation run.

Next, we must ensure that our telescope is oriented correctly. At BSUO, we point the telescope at a very bright, visible star in the sky, and after centering the star in our field of view, we can look up the star's exact coordinates in The

Astronomical Almanac, a yearly publication that lists current positions for hundreds of bright stars. At NURO, a dedicated positioning computer accurately and automatically calculates where the telescope is pointing, eliminating this step. Finally, the bright star is brought into focus. After this step, we are ready to begin data acquisition. We then take images of each targeted star with each of the four filters. The calibration frames are later used to correct each of the images taken throughout the night. Lists of targeted program stars, and observed "standard" stars are used to determine observed locations for each night.

## V. The Calcium Hydride Method

An efficient photometric system has been developed which permits discrimination between M-class giants and dwarfs using an intermediate-band Calcium Hydride filter (L) and standard Kron-Cousins system R and I magnitudes. Robertson and Furiak (1995) described the details of the development of this system.

In previous experiments, astronomers used blue (B) filters to plot blue-visual color index (B-V magnitudes) vs. visual-infrared color index (V-I magnitudes) for red stars. This diagram showed that dwarf and giant stars plotted on different areas of these graphs. This method can distinguish between dwarf and giant stars. The problem is that since we are dealing with faint red stars to begin with, it may be very difficult and time consuming to acquire an image using the blue filter. In addition, red dwarf stars having low atmospheric metal abundances can appear in the giant region of the B-V vs. V-I color diagrams. A

new method needed to be invented to speed the investigation of our targeted red stars.

The calcium hydride (CaH) photometry system is based on atmospheric density differences present in our target red star population. Red dwarfs, being smaller than giants, have higher density of gas in their outer atmospheres. The higher density gas present in red dwarf stars allows for a higher probability of molecule formation. Red giant stars have little calcium hydride present because their densities are not high enough for large amounts of calcium-hydrogen bonds to form (Maupin, 2002). Because red dwarf stars have higher concentrations of this molecule, their outer atmospheres absorb light at wavelengths specific to calcium hydride. Robertson selected CaH absorption bands centered at 638.5 nanometers in the spectra of red dwarfs (Robertson, 1984). This means that giants appear brighter at this particular wavelength, and Robertson developed a special filter to observe this, and thus enable us to determine the magnitude, or brightness of a star in this wavelength.

The CaH filter detects almost 6 times more flux than the blue filter for red stars. (Robertson, 2000) This is ideal for photometry on these faint red stars, which display very little flux in the blue filter region. CaH photometry reduces the total exposure time needed for faint red stars, as it takes a large exposure time with the blue filter to gather a high signal to noise ratio. This system allows faster, easier, and more reliable discrimination between red M-class giants and dwarfs, which is the goal of this project.

In 2000, the CaH-based method of luminosity classification successfully distinguished between red giant and red dwarf stars using a plot of instrumental L minus R magnitudes vs. a standardized R minus I magnitude. (Robertson and Scott, 2000) Again, R and I magnitudes are standardized to a standard system (known as the Kron-Cousins system). Also, since no standardized values have been established for the calcium hydride filter, thus instrumental magnitudes must be used. It was discovered that due to the absorption in the Calcium hydride filter (L), the L-R value was larger, and thus, red dwarfs appear in a distinct upper area of that graph, while red giants appear in a distinct lower region (Robertson and Scott, 2000).

## VI. Image Reduction – Standardized Magnitude Calculations:

Once images are collected, they must be processed. All image processing for this project was performed using the Image Reduction and Analysis Facility (IRAF) software of the National Optical Astronomy Observatories. This program runs in the UNIX environment which is maintained on a SUN Microsystem workstation housed in the Astronomy Research Center located in Cooper Science Building, Room 151.

The IRAF software task ZEROCOMBINE is used to average and combine bias frames into a master bias frame that is then subtracted pixel by pixel from each image. Then the FLATCOMBINE task makes an average of each flat field image that is made into a master flat field image for each filter. If images are taken from the BSUO, similar methods are used to combine the dark frames into

a single master frame. When viewing a star at different locations in the sky, you are looking through a different amount of air, which is termed airmass. IRAF calls a task SETAIRMASS that, using the observatory's location and along with the star's position, can compute the amount of airmass, or atmosphere, that the star is viewed through. This helps correct for atmospheric extinction of the starlight that the air causes. The CCDPROC task actually does the bias, dark and flat correction. After these steps, the images now contain the actual light received from the stars. Now IRAF is ready to do photometry (determination of the stellar brightness, or flux).

The IRAF tasks DIGIPHOT and DAOPHOT are also loaded to facilitate the photometry. Bright stars are automatically selected from each image using another task, DAOFIND, and exported to a list. The bright star list is used by IRAF to make individual measurements of brightness, or instrumental magnitude, for every selected star using the PHOT command. The magnitudes for each star are then exported to another list. When the software has measured the instrumental magnitudes, the program stars found in the selection task are identified using finding charts if the software has identified multiple bright stars. This is to ensure we are doing photometry on the target star and not a nearby neighbor of that star. The final list of targeted standard and program star magnitudes are combined in a list that IRAF will then fit to standardized star lists using transformation equations.

Observations of standard stars are used to compare to the catalog values, and with this comparison, a set of transformation equations is developed.

Standard stars are taken from the Landolt 1983 catalog. These stars are near the celestial equator, which allow easy observations from either hemisphere. Parameters are adjusted using IRAF's FITPARAMS task to find the best transformation equation parameters for the V, R, and I filters.

The equations below use several terms to transform the stars to the standard system. Figure 4 shows how the parameters, denoted by the filter name with a subscript, interact to transform the instrumentally determined magnitude into a magnitude on a standardized system. The first parameter is a zero point correction to account for differences between instrumentation at different observatories. The second term corrects for atmospheric light extinction, and the third parameter is for color bias in the filters. Terms four and five are second-order color corrections. Neither of these terms appears significant in our transformations. The sixth term corrects for any changes as a function of time throughout the night.

$$m_v = V + v_1 + v_2 XV + v_3 (V-R) + v_4 (V-R)XV + v_5 (V-R)^2 + v_6 tV$$
$$m_r = V - (V-R) + r_1 + r_2 XR + r_3 (V-R) + r_4 (V-R)XR + r_5 VR^2 + r_6 tR$$
$$m_I = V - (V-I) + i_1 + i_2 XI + i_3 (R-I) + r_4 (R-I)XI + i_5 VI^2 + i_6 tI$$

**Figure 4: Transformation Equations**

In Figure 4, XV, XR, XI stand for airmass value for each color image, t for time. V, R, and I stand for Visual, Red, and Infrared magnitudes, respectively, taken from the Kron-Cousins standardized list for each star. The m values are the instrumental magnitudes that IRAF calculates from our observations. After

inserting all of these values, the subscripted v, r and i terms are computed to achieve the best fit to the Kron-Cousins data.

Each filter has a unique transformation equation. These equations transform the V, R, and I instrumental magnitudes of the standard stars to the Kron-Cousins system, which give us standardized magnitudes. Next, an INVERTFIT task uses the transformation equations and parameters to transform the instrumental magnitudes of the program stars into magnitudes on the Kron-Cousins standard system also.

Notice that there is no transformation equation for the CaH (L) filter, which is not included on the Kron-Cousins system. We simply keep IRAF's instrumentally determined magnitude for our results. After the final transformation equations are applied, the data are ready to be graphed and analyzed. Importing the data to Microsoft Excel allows the data to be easily viewed and graphed.

## VII. Conclusions and Results

Nearly all (70 of 74) of our observed giant stars appear to be correctly classified as giant stars. Only two SAG stars show photometry more typical of dwarf stars than giants.

Figure 5 graphs the magnitude differences of (CaH-r) vs. (R-I) for program and standard stars observed to date. This chart shows distinct giant and dwarf sequences, separated by ~0.2 magnitudes. A sample of Maupin's confirmed SAD dwarfs is included. These known dwarfs are plotted to visually show where the dwarf sequence has been found to reside.

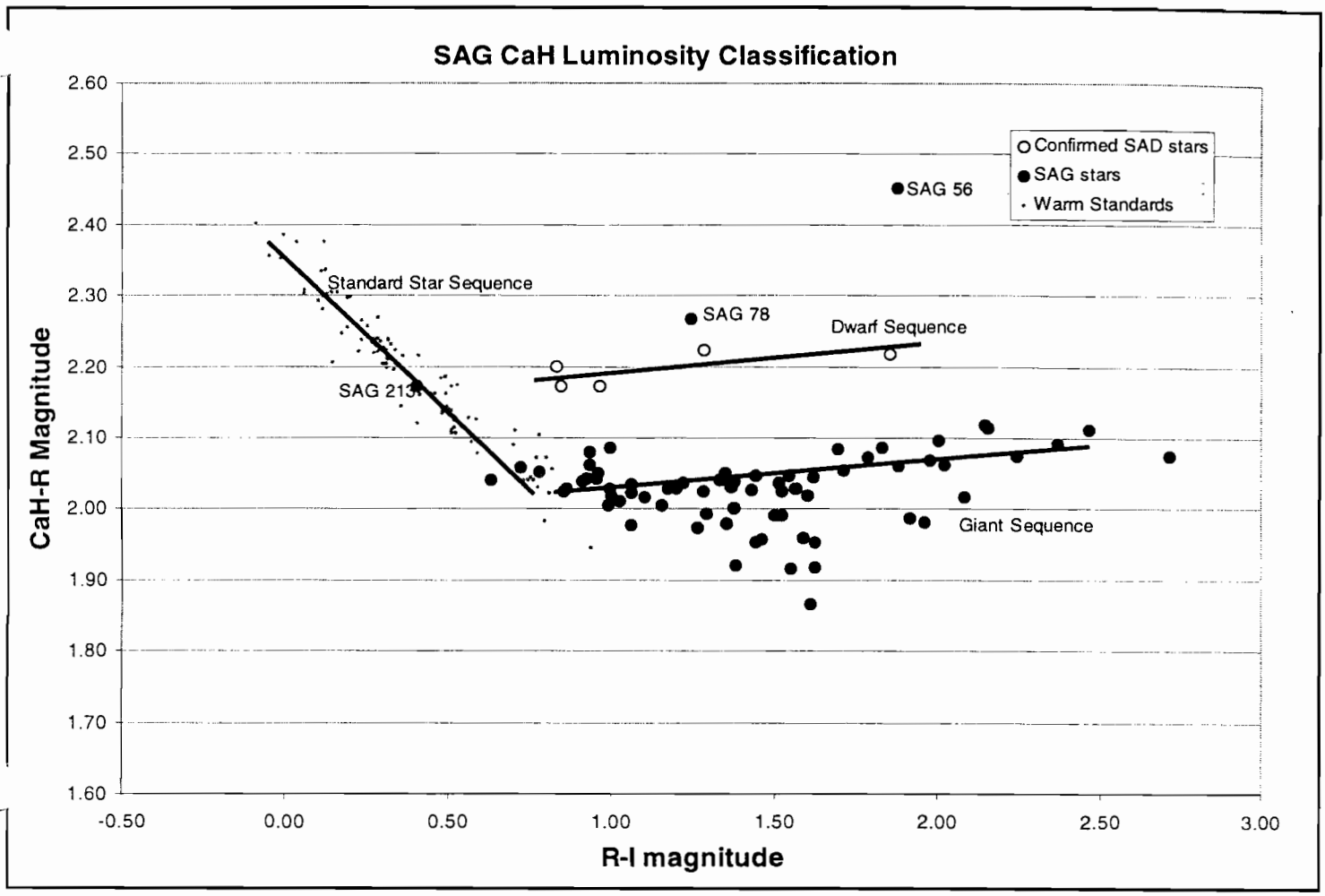


**Figure 5: Breakdown of Spectral Classifications of Observed SAG List**

This graph of instrumental CaH-R vs. R-I shows two distinct branches forming at R-I > ~0. 75. To the left of value, luminosity classes cannot be accurately determined, as the two sequences overlap. The difference in the standardized R and I values give a relative determination on how much red light the star emits. The difference in instrumental L and R values (L-R) give us the relative strength of the light emitted by the star in our CaH filter. Stars identified as dwarfs, which have strong absorption in the CaH filter region, should be fainter than their giant counterparts. Thus, they will have a higher color index

(instrumental L-R values). This is seen in the fact the in the instrumental L-R axis, dwarfs have a value considerably higher than giants do. This fact allows us to visually determine if our star is a dwarf or a giant.

Two SAG stars observed were outside the dwarf and giant sequence. SAG 213 has an R-I value of 0.40, which is an error, as a star with such a value would not be a red star. In Figure 5, SAG 213 clearly falls within the warmer standard star sequence. SAG 78 is not even shown in Figure 5, as the instrumental L-R value of 1.29 puts it far below the giant and dwarf sequences shown. Clearly, there is some source in error in these values. These stars will be the targets of subsequent observation runs.

The two dwarf stars detected have V magnitudes between 12 and 13. They are both between 10 and 20 degrees galactic latitude with one in each galactic hemisphere. One would expect that giant stars will be more frequent among the brighter stars and dwarf stars will be more frequent among the fainter stars at intermediate and high galactic latitudes (Matney, et al. 2004).

The remaining observed 70 SAG stars fall along the giant sequence and are most probably giant M stars. The temperature types do show a systematic trend in R-I as one would expect, although there is considerable overlap (Matney, et al. 2004). Figure 6 shows our giant confirmation results for a range of visual magnitudes.

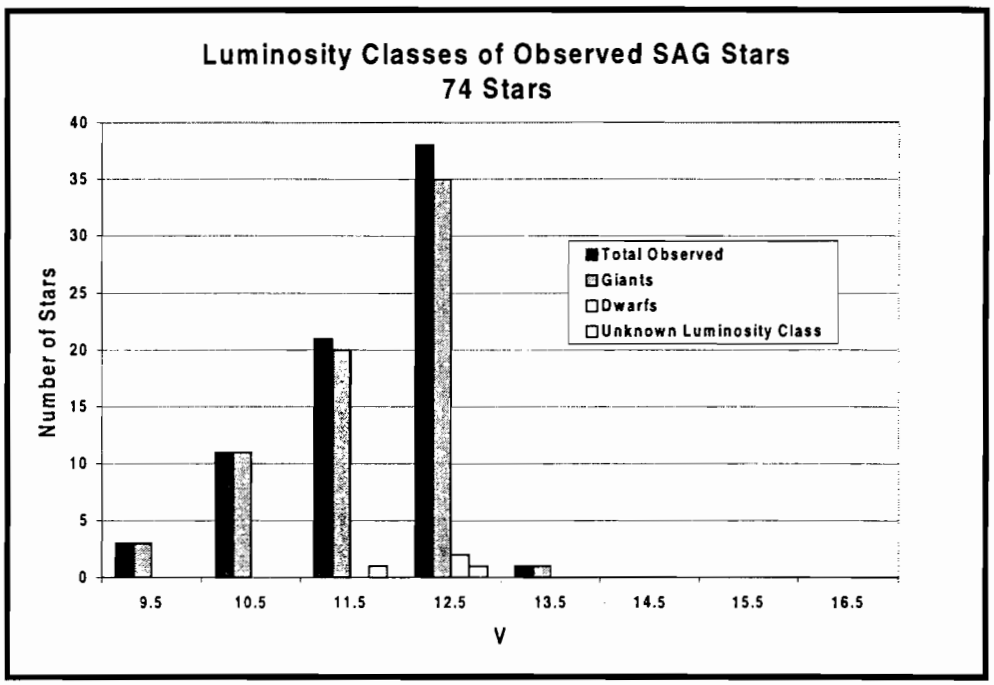


**Figure 6: Photometric Luminosity Classes of SAG Stars Observed to Date.**

Appendix B shows our combined data for all observed SAG program stars. The following table shows luminosity classes for the SAG stars sorted by visual magnitude. It also details which SAG stars have been identified as giants, dwarfs, and as of yet unconfirmed.

Of the previously observed SAD stars, many luminosity classification errors were found. Dexter (2003) has demonstrated that luminosity classes for spectral types earlier than K7 in this study are very unreliable. Maupin (2002) discovered more than half of his observed suspected dwarf stars are actually giants.

Of the SAG sample, the accuracy seems to be much higher, as only two observations of a possible dwarf have been noted. With the collected data, we can conclude that the initial luminosity classification of the SAG stars is much

more reliable than the SAD classifications. Table 2 shows a summary of the progress to date.

| SAG Program Stars | Number of Stars | Percent of Stars Observed |
|---|---|---|
| Total Number of Stars | 223 | |
| Stars Observed to Date | 74 | |
| Confirmed/Probable Dwarfs | 2 | 2.7% |
| Confirmed/Probable Giants | 70 | 94.6% |
| No Confirmation of L.C. | 2 | 2.7% |

**Table 2: Observational Results**

Clearly the success rate for determining luminosity classes for red giant stars is very good. For the four stars that were not verified as giants, only a single observation has been conducted of these stars. It is possible that subsequent observations will reveal an error during our observation or image reduction and reclassify the probable dwarfs and unclassifiable stars as giants. Additional observations will have to be scheduled to complete the remaining SAG stars. With only 30% of the SAG sample observed, we can note that the original luminosity classifications were almost 95% accurate.

# VIII. References


Dexter, M. (2003). Ball State University Master's Thesis (unpublished).

Krawchuck, C.A.P., P.C. Dawson, M.M. De Robertis. (2000). *Astron. J.*, **119**, 1956.

Landolt, A.U. (1983). *Astron. J.*, **88**, 439.

Landolt, A.U. (1992). *Astron. J.*, **104**, 340.

Matney J.E., et al., (2004). *B.A.A.S.* Vol. 36, No. 1. (abstract only).

Maupin, R. (2002). Ball State University Master's Thesis (unpublished).

"National Undergraduate Research Observatory". Northern Arizona University. Accessed November 30, 2004. < http:// http://www.nuro.nau.edu/nuro/info/filters.html>

Robertson, T.H. (1984). *Astron. J.*, **89**, 1229.

Robertson, T.H., (2000). In *The Kth Reunion*, A.G.D. Philip (ed.), pg. 35.

Robertson, T.H. and Furiak, N. (1995). B.A.A.S. Vol. 19, No. 1302. (abstract only)

Robertson, T.H. and Jordan, T. M., (1987). *B.A.A.S.* Vol. 19, No. 2, 703 (abstract only).

Robertson, T.H. and Scott, A. (2000). B.A.A.S. Vol. 32, No. 1392. (abstract only)

# Appendix A: Positions, Visual Magnitudes, and Spectral Types of SAG Program Stars

| | |
|---|---|
| **ID** | *SAG identification number* |
| **H** | *Hours of Right Ascension (R.A.)* |
| **M** | *Minutes of R.A.* |
| **S** | *Seconds of R.A.* |
| **d** | *Degrees of Declination (Dec.)* |
| **m** | *Minutes of Dec.* |
| **s** | *Seconds of Dec.* |
| **V** | *Visual magnitude* |
| **S.P.** | *Spectral class of star* |

| | RA | | | DEC | | | | |
|---|---|---|---|---|---|---|---|---|
| ID | H | M | S | d | m | s | V | SP. |
| SAG 1 | 0 | 53 | 16.1 | + 0 | 48 | 28 | 10.2 | M1 |
| SAG 2 | 2 | 53 | 26.4 | + 1 | 31 | 50 | 11.4 | M2 |
| SAG 3 | 3 | 51 | 15.8 | - 0 | 15 | 49 | 11.1 | M4 |
| SAG 4 | 3 | 52 | 43.8 | + 0 | 58 | 46 | 11.8 | M3 |
| SAG 5 | 4 | 48 | 4.1 | + 0 | 14 | 1 | 10.5 | M4 |
| SAG 6 | 4 | 53 | 5.9 | - 1 | 10 | 27 | 13.1 | M6 |
| SAG 7 | 4 | 55 | 2.5 | + 0 | 25 | 14 | 10.9 | M4 |
| SAG 8 | 4 | 55 | 26.5 | + 1 | 32 | 13 | 11.9 | M0 |
| SAG 9 | 4 | 56 | 44.0 | + 1 | 49 | 5 | 12.2 | M3 |
| SAG 10 | 4 | 56 | 50.1 | + 1 | 1 | 35 | 12.2 | M2 |
| SAG 11 | 4 | 56 | 58.3 | + 2 | 13 | 48 | 11.9 | K7 |
| SAG 12 | 4 | 57 | 6.2 | - 1 | 47 | 14 | 12.6 | M6 |
| SAG 13 | 4 | 59 | 49.2 | + 0 | 38 | 39 | 11.7 | M4 |
| SAG 14 | 5 | 0 | 11.5 | - 1 | 25 | 50 | 11.4 | M3 |
| SAG 15 | 5 | 0 | 18.4 | - 1 | 59 | 30 | 11.8 | M4 |
| SAG 16 | 5 | 0 | 52.8 | + 1 | 14 | 47 | 12.2 | M5 |
| SAG 17 | 5 | 3 | 28.0 | - 1 | 35 | 57 | 12.5 | M2 |
| SAG 18 | 5 | 4 | 34.5 | - 1 | 33 | 45 | 11.7 | M2 |
| SAG 19 | 5 | 4 | 37.2 | - 2 | 8 | 0 | 12.4 | M2 |
| SAG 20 | 5 | 5 | 28.1 | - 0 | 53 | 3 | 12.3 | M3 |
| SAG 21 | 5 | 5 | 49.4 | - 0 | 57 | 19 | 11.1 | M2 |
| SAG 22 | 5 | 53 | 31.2 | + 0 | 27 | 24 | 10.0 | M3 |
| SAG 23 | 5 | 54 | 40.3 | + 0 | 56 | 13 | 12.8 | M3 |
| SAG 24 | 5 | 55 | 11.7 | - 0 | 19 | 22 | 12.9 | M3 |
| SAG 25 | 5 | 55 | 49.5 | - 0 | 8 | 37 | 12.8 | M2 |
| SAG 26 | 5 | 55 | 56.9 | + 0 | 22 | 58 | 13.2 | M2 |
| SAG 27 | 5 | 56 | 1.3 | + 0 | 0 | 48 | 14.2 | M5 |
| SAG 28 | 5 | 56 | 1.2 | - 0 | 54 | 15 | 11.7 | M2 |
| SAG 29 | 5 | 56 | 18.3 | + 1 | 46 | 37 | 12.6 | M2 |
| SAG 30 | 5 | 57 | 1.4 | - 0 | 13 | 13 | 13.2 | M2 |
| SAG 31 | 5 | 57 | 5.6 | - 0 | 57 | 28 | 11.7 | M3 |
| SAG 32 | 5 | 58 | 11.5 | + 0 | 0 | 44 | 13.0 | M2 |
| SAG 33 | 5 | 58 | 40.2 | - 0 | 33 | 7 | 13.2 | M1 |
| SAG 34 | 5 | 59 | 26.7 | + 0 | 25 | 1 | 13.1 | M5 |
| SAG 35 | 5 | 59 | 33.4 | + 0 | 46 | 54 | 13.3 | M4 |
| SAG 36 | 5 | 59 | 33.4 | + 0 | 46 | 54 | 13.3 | M4 |
| SAG 37 | 5 | 59 | 34.1 | + 0 | 46 | 49 | 13.3 | M4 |
| SAG 38 | 5 | 59 | 34.1 | + 0 | 46 | 49 | 13.3 | M4 |
| SAG 39 | 5 | 59 | 52.2 | + 0 | 38 | 2 | 12.9 | M2 |
| SAG 40 | 6 | 0 | 23.5 | + 1 | 3 | 28 | 12.3 | M3 |
| SAG 41 | 6 | 0 | 22.4 | - 0 | 19 | 34 | 12.9 | M3 |
| SAG 42 | 6 | 0 | 47.9 | + 0 | 23 | 10 | 13.2 | M5 |
| SAG 43 | 6 | 48 | 12.2 | - 0 | 43 | 28 | 11.8 | M3 |
| SAG 44 | 6 | 48 | 41.4 | - 0 | 4 | 22 | 12.2 | M2 |
| SAG 45 | 6 | 48 | 51.6 | - 0 | 27 | 21 | 14.8 | M3 |
| SAG 46 | 6 | 49 | 5.3 | - 0 | 8 | 59 | 12.0 | M2 |
| SAG 47 | 6 | 49 | 45.5 | - 0 | 18 | 21 | 12.1 | M2 |
| SAG 48 | 6 | 52 | 35.0 | + 0 | 27 | 30 | 10.9 | M4 |
| SAG 49 | 6 | 53 | 15.8 | + 0 | 1 | 25 | 11.7 | M3 |
| SAG 50 | 6 | 53 | 22.9 | + 0 | 28 | 20 | 12.4 | M3 |

| | RA | | | DEC | | | | |
|---|---|---|---|---|---|---|---|---|
| ID | H | M | S | d | m | s | V | SP. |
| SAG 101 | 13 | 28 | 34.2 | - 1 | 5 | 57 | 12.1 | M4 |
| SAG 102 | 13 | 40 | 43.3 | + 1 | 53 | 4 | 9.8 | M4 |
| SAG 103 | 13 | 45 | 27.3 | + 0 | 12 | 11 | 9.7 | M3 |
| SAG 104 | 14 | 34 | 33.0 | - 1 | 40 | 52 | 12.8 | M2 |
| SAG 105 | 14 | 35 | 17.1 | - 0 | 59 | 22 | 10.3 | M4 |
| SAG 106 | 14 | 39 | 59.2 | - 2 | 26 | 47 | 9.9 | M4 |
| SAG 107 | 14 | 40 | 15.7 | + 1 | 8 | 25 | 11.1 | M4 |
| SAG 108 | 14 | 44 | 7.8 | + 0 | 57 | 7 | 11.0 | M4 |
| SAG 109 | 14 | 44 | 37.8 | + 0 | 22 | 21 | 11.0 | M2 |
| SAG 110 | 15 | 30 | 53.1 | - 0 | 25 | 35 | 11.0 | M4 |
| SAG 111 | 15 | 35 | 2.7 | + 0 | 0 | 54 | 10.7 | M3 |
| SAG 112 | 15 | 35 | 34.4 | + 0 | 48 | 48 | 11.8 | M3 |
| SAG 113 | 15 | 35 | 46.8 | - 1 | 49 | 12 | 12.3 | M3 |
| SAG 114 | 15 | 37 | 26.4 | + 0 | 18 | 38 | 11.1 | M4 |
| SAG 115 | 15 | 43 | 6.7 | - 1 | 30 | 22 | 12.2 | M4 |
| SAG 116 | 15 | 43 | 14.2 | + 1 | 44 | 37 | 12.4 | M4 |
| SAG 117 | 15 | 43 | 37.3 | - 1 | 42 | 33 | 10.8 | M5 |
| SAG 118 | 15 | 47 | 51.7 | - 1 | 21 | 35 | 12.1 | M3 |
| SAG 119 | 15 | 48 | 6.2 | + 1 | 19 | 14 | 11.8 | M4 |
| SAG 120 | 15 | 48 | 19.9 | - 0 | 14 | 19 | 11.1 | M4 |
| SAG 121 | 16 | 26 | 30.5 | + 0 | 35 | 42 | 12.4 | M3 |
| SAG 122 | 16 | 27 | 27.6 | - 1 | 28 | 50 | 12.2 | M5 |
| SAG 123 | 16 | 28 | 32.2 | - 1 | 4 | 14 | 12.7 | M5 |
| SAG 124 | 16 | 30 | 34.3 | + 1 | 13 | 51 | 11.4 | M3 |
| SAG 125 | 16 | 31 | 12.6 | + 0 | 18 | 8 | 14.9 | M1 |
| SAG 126 | 16 | 32 | 11.5 | - 1 | 38 | 1 | 10.7 | M5 |
| SAG 127 | 16 | 32 | 47.2 | + 0 | 14 | 4 | 13.1 | M5 |
| SAG 128 | 16 | 33 | 29.2 | - 0 | 15 | 36 | 14.3 | :M5 |
| SAG 129 | 16 | 34 | 44.0 | - 0 | 13 | 57 | 11.8 | M2 |
| SAG 130 | 16 | 34 | 46.4 | - 1 | 29 | 45 | 16.9 | M5 |
| SAG 131 | 16 | 36 | 37.7 | + 1 | 1 | 3 | 12.5 | M2 |
| SAG 132 | 16 | 37 | 1.4 | + 0 | 12 | 27 | 12.5 | M2 |
| SAG 133 | 16 | 39 | 31.2 | + 1 | 18 | 28 | 12.4 | M2 |
| SAG 134 | 16 | 39 | 32.1 | - 1 | 6 | 56 | 11.3 | M3 |
| SAG 135 | 16 | 39 | 43.6 | + 1 | 38 | 12 | 11.3 | M4 |
| SAG 136 | 16 | 39 | 57.1 | - 1 | 13 | 12 | 12.2 | M5 |
| SAG 137 | 16 | 40 | 7.5 | - 0 | 53 | 0 | 11.5 | M3 |
| SAG 138 | 16 | 42 | 9.5 | - 1 | 8 | 48 | 12.6 | M2 |
| SAG 139 | 16 | 42 | 53.1 | + 1 | 43 | 27 | 10.7 | M3 |
| SAG 140 | 16 | 43 | 43.5 | + 2 | 9 | 33 | 12.1 | M3 |
| SAG 141 | 16 | 44 | 4.7 | + 1 | 53 | 7 | 12.7 | M4 |
| SAG 142 | 16 | 44 | 38.1 | + 1 | 58 | 53 | 12.2 | M2 |
| SAG 143 | 16 | 45 | 12.0 | + 1 | 48 | 17 | 11.5 | M3 |
| SAG 144 | 17 | 41 | 51.1 | + 0 | 14 | 23 | 13.3 | M5 |
| SAG 145 | 17 | 41 | 56.3 | - 1 | 1 | 26 | 14.4 | M4 |
| SAG 146 | 17 | 42 | 53.2 | + 0 | 45 | 56 | 12.0 | :M1 |
| SAG 147 | 17 | 43 | 8.5 | + 0 | 7 | 30 | 11.0 | M3 |
| SAG 148 | 17 | 43 | 18.6 | + 0 | 27 | 9 | 12.4 | M3 |
| SAG 149 | 17 | 43 | 18.8 | + 0 | 27 | 14 | 12.4 | M3 |
| SAG 150 | 17 | 43 | 21.2 | - 0 | 16 | 14 | 13.2 | M5 |

| | RA | | | DEC | | | | |
|---|---|---|---|---|---|---|---|---|
| ID | H | M | S | d | m | s | V | SP. |
| SAG 151 | 17 | 43 | 21.7 | - 0 | 16 | 19 | 13.2 | M5 |
| SAG 152 | 17 | 43 | 34.3 | - 0 | 0 | 40 | 13.3 | M5 |
| SAG 153 | 17 | 43 | 52.8 | - 0 | 59 | 2 | 11.7 | M3 |
| SAG 154 | 17 | 44 | 5.6 | - 0 | 4 | 21 | 12.7 | M3 |
| SAG 155 | 17 | 44 | 30.3 | + 0 | 37 | 33 | 12.1 | M3 |
| SAG 156 | 17 | 44 | 29.7 | - 0 | 22 | 37 | 12.7 | M3 |
| SAG 157 | 17 | 45 | 35.3 | - 0 | 0 | 58 | 12.1 | M3 |
| SAG 158 | 17 | 45 | 49.5 | - 0 | 37 | 12 | 12.3 | M2 |
| SAG 159 | 17 | 46 | 18.9 | - 0 | 12 | 3 | 13.1 | M3 |
| SAG 160 | 17 | 46 | 21.0 | + 0 | 28 | 1 | 11.4 | M4 |
| SAG 161 | 17 | 46 | 21.4 | - 0 | 54 | 37 | 12.3 | M3 |
| SAG 162 | 17 | 46 | 26.0 | + 0 | 15 | 23 | 12.2 | M3 |
| SAG 163 | 17 | 46 | 29.8 | + 0 | 43 | 3 | 12.6 | M4 |
| SAG 164 | 17 | 46 | 39.2 | - 0 | 48 | 55 | 13.6 | M3 |
| SAG 165 | 17 | 47 | 44.7 | + 0 | 17 | 54 | 12.3 | M3 |
| SAG 166 | 17 | 47 | 51.4 | + 0 | 19 | 26 | 12.0 | M1 |
| SAG 167 | 17 | 48 | 3.5 | - 0 | 41 | 11 | 12.4 | M5 |
| SAG 168 | 17 | 49 | 1.6 | - 0 | 50 | 45 | 13.1 | M3 |
| SAG 169 | 18 | 40 | 18.2 | - 0 | 33 | 41 | 13.6 | M3 |
| SAG 170 | 18 | 46 | 10.3 | + 0 | 18 | 16 | 11.3 | M4 |
| SAG 171 | 19 | 34 | 53.0 | - 0 | 29 | 25 | 12.5 | M4 |
| SAG 172 | 19 | 35 | 16.4 | - 0 | 24 | 45 | 12.6 | M3 |
| SAG 173 | 19 | 35 | 26.0 | + 0 | 42 | 49 | 14.8 | M5 |
| SAG 174 | 19 | 35 | 35.4 | + 0 | 31 | 42 | 12.4 | M3 |
| SAG 175 | 19 | 35 | 39.8 | + 0 | 14 | 41 | 11.8 | M3 |
| SAG 176 | 19 | 35 | 45.4 | - 0 | 26 | 39 | 12.6 | M3 |
| SAG 177 | 19 | 35 | 57.3 | - 0 | 5 | 30 | 10.9 | M3 |
| SAG 178 | 19 | 37 | 2.1 | + 0 | 55 | 29 | 13.0 | M4 |
| SAG 179 | 19 | 37 | 34.2 | + 0 | 29 | 32 | 13.8 | M5 |
| SAG 180 | 19 | 37 | 39.2 | + 0 | 38 | 10 | 13.1 | M5 |
| SAG 181 | 19 | 37 | 38.7 | - 0 | 5 | 48 | 13.1 | M3 |
| SAG 182 | 19 | 37 | 57.4 | - 0 | 18 | 45 | 12.3 | M3 |
| SAG 183 | 19 | 38 | 17.9 | + 1 | 6 | 9 | 12.4 | M4 |
| SAG 184 | 19 | 38 | 31.6 | + 0 | 50 | 26 | 12.0 | M3 |
| SAG 185 | 19 | 38 | 33.8 | - 0 | 31 | 31 | 12.4 | M4 |
| SAG 186 | 19 | 39 | 21.0 | + 0 | 59 | 10 | 12.9 | M3 |
| SAG 187 | 19 | 39 | 21.6 | + 0 | 4 | 46 | 12.5 | M3 |
| SAG 188 | 19 | 39 | 42.5 | + 1 | 13 | 14 | 12.4 | M4 |
| SAG 189 | 19 | 39 | 44.9 | + 0 | 41 | 38 | 12.7 | M4 |
| SAG 190 | 19 | 40 | 4.9 | - 0 | 37 | 59 | 11.8 | M4 |
| SAG 191 | 19 | 40 | 21.9 | + 0 | 50 | 47 | 11.7 | M3 |
| SAG 192 | 19 | 40 | 29.9 | - 0 | 1 | 31 | 12.7 | M3 |
| SAG 193 | 19 | 40 | 32.3 | - 0 | 18 | 6 | 12.8 | M2 |
| SAG 194 | 19 | 40 | 40.0 | + 1 | 8 | 52 | 12.8 | M2 |
| SAG 195 | 19 | 40 | 44.6 | + 1 | 0 | 17 | 12.2 | M3 |
| SAG 196 | 19 | 40 | 44.5 | + 0 | 43 | 3 | 13.3 | M3 |
| SAG 197 | 19 | 40 | 48.8 | + 1 | 16 | 22 | 12.4 | M3 |
| SAG 198 | 19 | 40 | 57.9 | + 0 | 12 | 32 | 12.8 | M4 |
| SAG 199 | 19 | 41 | 37.0 | + 1 | 1 | 6 | 12.7 | M2 |
| SAG 200 | 19 | 41 | 36.4 | + 0 | 8 | 56 | 11.6 | M4 |

| | RA | | | DEC | | | | |
|---|---|---|---|---|---|---|---|---|
| ID | H | M | S | d | m | s | V | SP. |
| SAG 201 | 19 | 42 | 3.4 | - 0 | 2 | 24 | 10.7 | M2 |
| SAG 202 | 19 | 42 | 13.6 | + 1 | 7 | 57 | 11.9 | M3 |
| SAG 203 | 19 | 42 | 17.5 | + 0 | 56 | 27 | 13.1 | M3 |
| SAG 204 | 19 | 42 | 24.5 | + 0 | 57 | 16 | 12.7 | M2 |
| SAG 205 | 19 | 42 | 26.4 | + 1 | 5 | 48 | 12.3 | M4 |
| SAG 206 | 20 | 39 | 57.5 | - 0 | 6 | 20 | 13.1 | M4 |
| SAG 207 | 20 | 40 | 53.9 | + 1 | 11 | 11 | 10.5 | M4 |
| SAG 208 | 20 | 41 | 3.3 | + 0 | 1 | 16 | 12.7 | M3 |
| SAG 209 | 20 | 41 | 22.5 | + 0 | 50 | 23 | 13.7 | M5 |
| SAG 210 | 20 | 41 | 53.6 | - 0 | 0 | 7 | 12.7 | M2 |
| SAG 211 | 20 | 42 | 9.4 | + 0 | 5 | 22 | 13.0 | M3 |
| SAG 212 | 20 | 43 | 9.0 | + 1 | 23 | 6 | 13.8 | M3 |
| SAG 213 | 20 | 43 | 43.0 | - 0 | 6 | 8 | 11.6 | M4 |
| SAG 214 | 20 | 44 | 55.1 | + 0 | 57 | 40 | 11.9 | M4 |
| SAG 215 | 20 | 45 | 8.3 | - 0 | 16 | 40 | 12.9 | M5 |
| SAG 216 | 20 | 45 | 18.0 | + 1 | 20 | 43 | 12.8 | M3 |
| SAG 217 | 20 | 46 | 34.4 | - 0 | 13 | 25 | 12.3 | M4 |
| SAG 218 | 21 | 41 | 48.5 | - 0 | 11 | 10 | 11.6 | M4 |
| SAG 219 | 21 | 43 | 50.2 | + 0 | 56 | 37 | 11.7 | M3 |
| SAG 220 | 21 | 44 | 56.8 | + 1 | 18 | 43 | 11.4 | M3 |
| SAG 221 | 21 | 45 | 57.7 | + 0 | 37 | 1 | 11.3 | M3 |
| SAG 222 | 21 | 45 | 58.7 | + 0 | 37 | 1 | 11.3 | M3 |
| SAG 223 | 23 | 44 | 4.2 | + 0 | 22 | 52 | 11.6 | M4 |

# Appendix B: Completed Observational Data of SAG list

| | |
|---|---|
| **ID** | *SAG identification number* |
| **V** | *Visual magnitude* |
| **<R-I>** | *Mean difference in standardized R minus I values* |
| **<I-r>** | *Mean difference in instrumental L minus R values* |
| **# Obs** | *Number of observations recorded for star* |
| **Spec Type** | *Spectral class of star* |

| ID | V | <R-I> | <I-r> | # Obs | Spec Type |
|---|---|---|---|---|---|
| Confirmed/Probable Giants | | | | | |
| SAG 1 | 10.2 | 0.93 | 2.08 | 2 | M1 |
| SAG 2 | 11.4 | 1.06 | 2.04 | 2 | M2 |
| SAG 3 | 11.1 | 2.71 | 2.07 | 1 | M4 |
| SAG 4 | 11.8 | 1.56 | 2.03 | 1 | M3 |
| SAG 6 | 13.1 | 2.37 | 2.09 | 1 | M6 |
| SAG 8 | 11.9 | 0.86 | 2.03 | 2 | M0 |
| SAG 9 | 12.2 | 1.00 | 2.02 | 1 | M3 |
| SAG 10 | 12.2 | 0.85 | 2.02 | 1 | M2 |
| SAG 11 | 11.9 | 0.78 | 2.05 | 1 | K7 |
| SAG 12 | 12.6 | 2.46 | 2.11 | 1 | M6 |
| SAG 13 | 11.7 | 1.62 | 2.04 | 1 | M4 |
| SAG 14 | 11.4 | 1.17 | 2.03 | 1 | M3 |
| SAG 15 | 11.8 | 1.57 | 2.03 | 1 | M4 |
| SAG 16 | 12.2 | 1.88 | 2.06 | 1 | M5 |
| SAG 17 | 12.5 | 1.03 | 2.01 | 1 | M2 |
| SAG 18 | 11.7 | 0.99 | 2.01 | 1 | M2 |
| SAG 19 | 12.4 | 1.00 | 2.03 | 1 | M2 |
| SAG 20 | 12.3 | 1.37 | 2.04 | 1 | M3 |
| SAG 23 | 12.8 | 1.96 | 1.98 | 1 | M3 |
| SAG 24 | 12.9 | 1.55 | 1.92 | 1 | M3 |
| SAG 25 | 12.8 | 1.63 | 1.92 | 1 | M2 |
| SAG 31 | 11.7 | 1.50 | 1.99 | 1 | M3 |
| SAG 39 | 12.9 | 1.38 | 1.92 | 1 | M2 |
| SAG 40 | 12.3 | 2.08 | 2.02 | 1 | M3 |
| SAG 41 | 12.9 | 1.62 | 1.95 | 1 | M3 |
| SAG 44 | 12.2 | 1.44 | 1.95 | 2 | M2 |
| SAG 47 | 12.1 | 1.46 | 1.96 | 2 | M2 |
| SAG 48 | 10.9 | 1.92 | 1.99 | 1 | M4 |
| SAG 50 | 12.4 | 1.59 | 1.96 | 1 | M3 |
| SAG 51 | 12.3 | 1.61 | 1.87 | 2 | M3 |
| SAG 52 | 12.6 | 2.02 | 2.06 | 1 | M5 |
| SAG 54 | 10.8 | 0.91 | 2.04 | 1 | M2 |
| SAG 55 | 12.0 | 1.22 | 2.04 | 1 | M3 |
| SAG 57 | 12.0 | 1.54 | 2.05 | 1 | M4 |
| SAG 58 | 11.1 | 0.72 | 2.06 | 1 | M1 |
| SAG 59 | 10.1 | 1.33 | 2.04 | 2 | M4 |
| SAG 60 | 11.3 | 1.71 | 2.06 | 1 | M4 |
| SAG 61 | 11.4 | 1.51 | 2.04 | 1 | M4 |
| SAG 62 | 11.4 | 1.52 | 2.02 | 2 | M4 |
| SAG 63 | 11.3 | 1.00 | 2.09 | 1 | M2 |
| SAG 64 | 10.9 | 1.20 | 2.03 | 1 | M4 |
| SAG 65 | 12.6 | 0.63 | 2.04 | 1 | M4 |
| SAG 68 | 12.7 | 0.95 | 2.04 | 1 | M3 |
| SAG 69 | 11.5 | 1.79 | 2.07 | 1 | M4 |
| SAG 70 | 10.2 | 1.43 | 2.03 | 1 | M4 |
| SAG 72 | 9.6 | 1.44 | 2.05 | 1 | M4 |
| SAG 74 | 9.8 | 2.24 | 2.07 | 1 | M4 |
| SAG 75 | 10.6 | 0.93 | 2.06 | 1 | M3 |
| SAG 77 | 10.7 | 1.36 | 2.04 | 1 | M4 |

| ID | V | <R-I> | <I-r> | # Obs | Spec Type |
|---|---|---|---|---|---|
| SAG 79 | 9.9 | 1.37 | 2.03 | 1 | M4 |
| SAG 80 | 10.5 | 0.93 | 2.04 | 1 | M3 |
| SAG 81 | 12.0 | 2.15 | 2.11 | 1 | M5 |
| SAG 82 | 10.5 | 0.96 | 2.05 | 1 | M3 |
| SAG 83 | 10.2 | 1.69 | 2.09 | 1 | M4 |
| SAG 171 | 12.5 | 1.98 | 2.07 | 2 | M4 |
| SAG 176 | 12.6 | 1.52 | 1.99 | 1 | M3 |
| SAG 193 | 12.8 | 1.38 | 2.00 | 1 | M2 |
| SAG 194 | 12.8 | 1.27 | 1.97 | 2 | M2 |
| SAG 198 | 12.8 | 1.60 | 2.02 | 1 | M4 |
| SAG 199 | 12.7 | 1.29 | 1.99 | 1 | M2 |
| SAG 204 | 12.7 | 1.35 | 1.98 | 1 | M2 |
| SAG 208 | 12.7 | 1.06 | 1.98 | 2 | M3 |
| SAG 210 | 12.7 | 1.16 | 2.00 | 1 | M2 |
| SAG 214 | 11.9 | 1.28 | 2.03 | 1 | M4 |
| SAG 215 | 12.9 | 2.00 | 2.10 | 1 | M5 |
| SAG 216 | 12.8 | 1.35 | 2.05 | 1 | M3 |
| SAG 217 | 12.3 | 2.15 | 2.12 | 1 | M4 |
| SAG 218 | 11.6 | 1.83 | 2.09 | 2 | M4 |
| SAG 219 | 11.7 | 1.06 | 2.02 | 1 | M3 |
| SAG 220 | 11.4 | 1.10 | 2.02 | 1 | M3 |
| Confirmed/Probable Dwarfs | | | | | |
| SAG 29 | 12.6 | 1.24 | 2.27 | 1 | M2 |
| SAG 56 | 12.9 | 1.88 | 2.45 | 1 | M4 |
| Unconfirmed | | | | | |
| SAG 78 | 12.5 | 1.76 | **1.29** | 1 | M5 |
| SAG 213 | 11.6 | **0.40** | 2.17 | 1 | M4 |